A Mechanism Displaying Autocatalysis: The Hydrogenation of Acetophenone Catalyzed by RuH(*S*-binap)(app) Where app Is the Amido Ligand Derived from 2-Amino-2-(2-pyridyl)propane

Alen Hadzovic, Datong Song, Christina M. MacLaughlin, and Robert H. Morris*

Davenport Laboratory, Department of Chemistry, University of Toronto, 80 St. George Street, Toronto, Ontario M5S 3H6, Canada

Received August 23, 2007

The 2-(aminomethyl)pyridine (ampy) ligand is known to activate ruthenium complexes for the catalytic hydrogenation of ketones. Here we prepare well-defined catalysts using the new ligand 2-amino-2-(2-pyridyl)propane (appH) in order to elucidate the role of the pyridyl group. The ligand has two methyl groups on the α-carbon to block β-hydride elimination reactions. It reacts with RuHCl(*S*-binap)(PPh_3) to produce the orange-yellow complex RuHCl(*S*-binap)(appH) (**2**). In the presence of a strong base (KO^t-Bu), complex **2** is converted into an active catalyst for the H_2-hydrogenation of acetophenone in benzene under mild conditions (20 °C, 5 atm H_2). Solutions of **2** rapidly react with KO^tBu under an argon atmosphere to produce a deep red amidohydrido complex RuH(*S*-binap)(app) (**3**), which is an active catalyst. A crystal structure determination of **3** represents the first structure of a Ru-binap hydrido-amido complex. It reveals a five-coordinate Ru(II) center with a short Ru−N(amido) distance (1.962(3) Å) and a trigonal planar geometry at the amido nitrogen. The kinetic experiments using **3** as a catalyst and acetophenone as a substrate in benzene show that the rate of 1-phenylethanol production is dependent on both catalyst and H_2 concentrations. These results parallel the behavior of the conventional Noyori-type Ru(II) catalysts with diamine ligands. However, unique features of catalysis with **3** are as follows: (1) the formation of a dihydride is thermodynamically unfavorable at 1 atm H_2, 20 °C; (2) the rate shows a dependence on the product concentration since it increases as the product builds up during the reaction in an autocatalytic fashion. A significant increase in the initial rate is observed when a critical concentration of *rac*-1-phenylethanol is present at the beginning of the reaction. The addition of 2-propanol in benzene raises the rate as well, and the fastest H_2-hydrogenation is achieved if 2-propanol is used as a solvent. This "alcohol effect" is favored by the pyridyl ligand app since it was not observed for the similar catalyst RuH($NHCMe_2CMe_2NH_2$)(binap). While **3** is an exceptional catalyst for H_2-hydrogenation in 2-propanol (TOF > 6700 h^{-1} at 20 °C, 5 atm H_2), it has a lower activity in transfer hydrogenation from the same solvent under comparable conditions (TOF 110 h^{-1} at 20 °C, 1 atm Ar). DFT calculations on the model amido complex Ru(H)(PH_3)$_2$($HNCH_2C_5H_4N$) (**4**) confirm that the splitting of H_2 to give the trans dihydride is the turnover-limiting step and lies 9 kcal/mol in free energy above the transition state for the ketone hydrogenation step. The formation of the dihydride is entropically unfavorable. The theoretical activation barrier for H_2 splitting is lowered by 5 kcal/mol by an alcohol-assisted mechanism but still remains higher in energy than the ketone hydrogenation step. This latter step can also be alcohol-assisted and can result in a different ee in the product alcohol than without alcohol assistance, as observed experimentally for reactions using 2-propanol versus benzene as the solvent. With alcohol present, an alkoxohydridoruthenium(II) complex is calculated to be the catalyst resting state.

Introduction

Transition metal amido complexes play an important role in both catalysis (as catalysts and/or intermediates in catalysis) and stoichiometric reactions.[1−3] For example, they function as strong bases in stoichiometric carbon−hydrogen bond activation reactions,[4−6] dihydrogen splitting,[7] and insertion reactions into the amido N−H bond.[4,8,9] They have been recognized as intermediates in amination and hydroamination of arylhalides.[10,11] Ruthenium amido complexes have featured prominently as active catalysts or catalyst intermediates in hydrogenation[7,12−20] and transfer hydrogenation[16,21−24] of ketones and in

* Corresponding author. E-mail: rmorris@chem.utoronto.ca.

(1) Fryzuk, M. D.; Montgomery, C. D. *Coord. Chem. Rev.* **1989**, *95*, 1−40.
(2) Fulton, J. R.; Holland, A. W.; Fox, D. J.; Bergman, R. G. *Acc. Chem. Res.* **2002**, *35*, 44−56.
(3) Gunnoe, T. B. *Eur. J. Inorg. Chem.* **2007**, 1185−1203.
(4) Fulton, J. R.; Bouwkamp, M. W.; Bergman, R. G. *J. Am. Chem. Soc.* **2000**, *122*, 8799−8800.
(5) Eckert, N. A.; Smith, J. M.; Lachicotte, R. J.; Holland, P. L. *Inorg. Chem.* **2004**, *43*, 3306 -3321.
(6) Feng, Y.; Lail, M.; Foley, N. A.; Gunnoe, T. B.; Barakat, K. A.; Cundari, T. R.; Petersen, J. L. *J. Am. Chem. Soc.* **2006**, *128*, 7982−7994.
(7) Abdur-Rashid, K.; Faatz, M.; Lough, A. J.; Morris, R. H. *J. Am. Chem. Soc.* **2001**, *123*, 7473−7474.
(8) Rais, D.; Bergman, R. G. *Chem.−Eur. J.* **2004**, *10*, 3970 - 3978.
(9) Fox, D. J.; Bergman, R. G. *J. Am. Chem. Soc.* **2003**, *125*, 8984−8985.
(10) Hartwig, J. F.; Richards, S.; Baranano, D.; Paul, F. *J. Am. Chem. Soc.* **1996**, *118*, 3626−3633.
(11) Alcazar-Roman, L. M.; Hartwig, J. F.; Rheingold, A. L.; Liable-Sands, L. M.; Guzei, I. A. *J. Am. Chem. Soc.* **2000**, *122*, 4618−4630.
(12) Noyori, R.; Ohkuma, T. *Angew. Chem., Int. Ed.* **2001**, *40*, 40−73.

10.1021/om700849w CCC: $37.00
Publication on Web 10/20/2007

Scheme 1. β-Hydride Elimination from an Amido Ligand

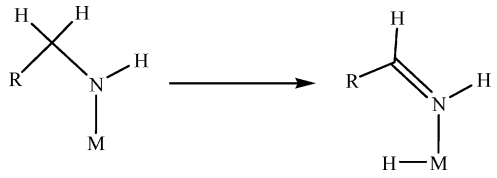

conjugate addition reactions.[24−26]

A major concern in the preparation of coordinatively unsaturated transition metal amido complexes is their ability to undergo β-hydride elimination from the carbon backbone of the ligand, generating a hydrido-imine complex (Scheme 1).[7,10,27,28] In order to overcome this problem, ligands without hydrogen atoms on carbon α to the nitrogen donor have been used. The earliest examples of such ligands include $N(SiMe_3)_2^-$, $NHPh^-$, and NPh_2^-.[1] Other, more elaborate mono- and polydentate ligands followed.[29,30]

Our group has reported the isolation and characterization of Ru(II) amido complexes $Ru(H)(P_2)(H_2NCMe_2CMe_2NH)$, P_2 = *R*-binap or $(PPh_3)_2$,[7,13] that have an amido ligand with the α-positions blocked with methyl groups. These complexes proved to constitute a part of a catalytic cycle for hydrogenation of ketones to alcohols in Noyori-type catalytic systems (Scheme 2). In this cycle, the hydridoamido complex heterolytically cleaves the H_2 molecule over the Ru−N amido bond to produce a trans dihydride amine species. The trans dihydride complex that is formed in this way transfers a hydride and a proton (an equivalent of H_2) to the carbonyl group of the ketone to produce alcohol and regenerates the hydridoamido complex. This catalytic cycle explains well the diamine or "N−H effect" previously observed by Noyori and co-workers.[22,31] Similar hydrido-amido complexes, derived from nonblocked diamines, proved to be unstable and could be observed only in certain NMR experiments along with their decomposition products.[32,33]

Scheme 2. Proposed Mechanism of Action of Ruthenium Hydridoamine Complexes in the Catalytic Hydrogenation of Ketones

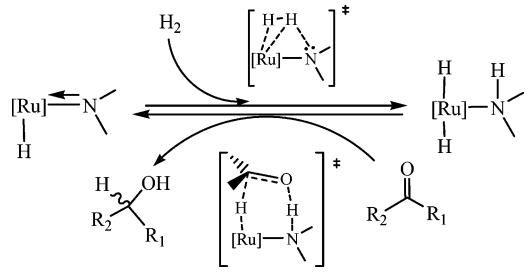

There are several reports in the recent literature of an increased catalytic activity of ketone hydrogenation catalysts when a conventional diamine ligand is replaced with 2-(aminomethyl)pyridine (ampy). Noyori and co-workers have observed that RuXY(*S*-tolbinap)(ampy) (X, Y = Cl; X = H, Y = BH_4) are excellent (pre)catalysts for hydrogenation of bulky, deactivated *tert*-alkyl ketones for which typical RuX_2-(diphosphine)(diamine) catalysts are less effective.[34] This increased activity of ampy over diamine catalysts has been explained by the presence of a flat pyridine ring that lowers a nonbonding repulsion between the incoming substrate and the backbone of the catalyst. Baratta and co-workers developed the catalyst precursors $RuCl_2$(diphosphine)(ampy)[35] and RuCl-(CNN)(diphosphine), where CNN is 6-(4′-methylphenyl)-2-pyridylmethylamine, a tridentate ligand forming orthometalated Ru(II) complexes.[36] These are remarkably active in transfer hydrogenation of ketones from 2-propanol at elevated temperatures. We have described *trans*-$RuHCl(PPh_3)_2$(ampy) and *cis*,*cis*-$Ru(H)_2(PPh_3)_2$(ampy), precursors to the catalyst system that is much more active in the H_2-hydrogenation of acetophenone than those obtained from related complexes *trans*-$RuHCl(PPh_3)_2$-(*R*,*R*-dach) and *cis*,*cis*-$Ru(H)_2(PPh_3)_2$(*R*,*R*-dach) (*R*,*R*-dach = 1*R*,2*R*-diaminocyclohexane).[32]

Some of us previously designed the ligand 2-phenyl-6-(2-aminoisopropyl)pyridine, with methyl groups on the α-carbon of the amino group to allow the synthesis of stable Pd and Pt amido compounds.[37] Here we report the preparation of the novel ligand 2-amino-2-(2-pyridyl)propane (appH), an analogue of ampy with two methyl groups on the carbon α to the amine. This ligand design enables the isolation of the Ru(II) hydridoamido complex RuH(*S*-binap)(app) and its full characterization. The other known complex of this type, RuH(*R*-binap)($NHCMe_2$-CMe_2NH_2), has not been isolated in a crystalline form.[7] This provides us with a well-defined catalytic system to study and model with DFT calculations.

Results and Discussion

Synthesis of the appH Ligand. The ligand was prepared according to Scheme 3 following a route based partly on the previously reported synthesis of 2-aminomethyl-6-phenylpyridine.[37] Refluxing the alcohol **1a** in a mixture of CH_3CN/BF_3-

(13) Abdur-Rashid, K.; Clapham, S. E.; Hadzovic, A.; Harvey, J. N.; Lough, A. J.; Morris, R. H. *J. Am. Chem. Soc.* **2002**, *124*, 15104−15118.
(14) Sandoval, C. A.; Ohkuma, T.; Muñiz, K.; Noyori, R. *J. Am. Chem. Soc.* **2003**, *125*, 13490−13503.
(15) Clapham, S. E.; Hadzovic, A.; Morris, R. H. *Coord. Chem. Rev.* **2004**, *248*, 2201−2237.
(16) Muñiz, K. *Angew. Chem., Int. Ed.* **2005**, *44*, 6622−6627.
(17) Clapham, S. E.; Morris, R. H. *Organometallics* **2005**, *24*, 479−481.
(18) Sandoval, C. A.; Ohkuma, T.; Utsumi, N.; Tsutsumi, K.; Murata, K.; Noyori, R. *Chem. Asian J.* **2006**, *1*, 102−110.
(19) Hamilton, R. J.; Bergens, S. H. *J. Am. Chem. Soc.* **2006**, *128*, 13700−13701.
(20) Ohkuma, T.; Tsutsumi, K.; Utsumi, N.; Arai, N.; Noyori, R.; Murata, K. *Org. Lett.* **2007**, *9*, 255−257.
(21) Haack, K. J.; Hashiguchi, S.; Fujii, A.; Ikariya, T.; Noyori, R. *Angew. Chem., Int. Ed. Engl.* **1997**, *36*, 285−288.
(22) Yamakawa, M.; Ito, H.; Noyori, R. *J. Am. Chem. Soc.* **2000**, *122*, 1466−1478.
(23) Boubekeur, L.; Ulmer, S.; Ricard, L.; Mezailles, N.; LeFloch, P. *Organometallics* **2006**, *25*, 315−317.
(24) Ikariya, T.; Murata, K.; Noyori, R. *Org. Biomol. Chem.* **2006**, *4*, 393−406.
(25) Watanabe, M.; Ikagawa, A.; Wang, H.; Murata, K.; Ikariya, T. *J. Am. Chem. Soc.* **2004**, *126*, 11148−11149.
(26) Clapham, S. E.; Guo, R.; Zimmer-DeIuliis, M.; Rasool, N.; Lough, A.; Morris, R. H. *Organometallics* **2006**, *25*, 5477−5486.
(27) Diamond, S. E.; Mares, F. *J. Organomet. Chem.* **1977**, *142*, C55 - C57.
(28) Hartwig, J. F. *J. Am. Chem. Soc.* **1996**, *118*, 7010−7011.
(29) Cooper, M. K.; Downes, J. M. *Inorg. Chem.* **1978**, *17*, 880−884.
(30) Fryzuk, M. D.; MacNeil, P. A.; Rettig, S. J.; Secco, A. S.; Trotter, J. *Organometallics* **1982**, *1*, 918 - 930.
(31) Ohkuma, T.; Ooka, H.; Hashiguchi, S.; Ikariya, T.; Noyori, R. *J. Am. Chem. Soc.* **1995**, *117*, 2675−2676.
(32) Abdur-Rashid, K.; Abbel, R.; Hadzovic, A.; Lough, A. J.; Morris, R. H. *Inorg. Chem.* **2005**, *44*, 2483−2492.
(33) Abbel, R.; Abdur-Rashid, K.; Faatz, M.; Hadzovic, A.; Lough, A. J.; Morris, R. H. *J. Am. Chem. Soc.* **2005**, *127*, 1870−1882.
(34) Ohkuma, T.; Sandoval, C. A.; Srinivasan, R.; Lin, Q.; Wei, Y.; Muñiz, K.; Noyori, R. *J. Am. Chem. Soc.* **2005**, *127*, 8288−8289.
(35) Baratta, W.; Herdtweck, E.; Siega, K.; Toniutti, M.; Rigo, P. *Organometallics* **2005**, *24*, 1660−1669.
(36) Baratta, W.; Chelucci, G.; Gladiali, S.; Siega, K.; Toniutti, M.; Zanette, M.; Zangrando, E.; Rigo, P. *Angew. Chem., Int. Ed.* **2005**, *44*, 6214−6219.
(37) Song, D.; Morris, R. H. *Organometallics* **2004**, *23*, 4406−4413.

Scheme 3. Preparation of the appH Ligand

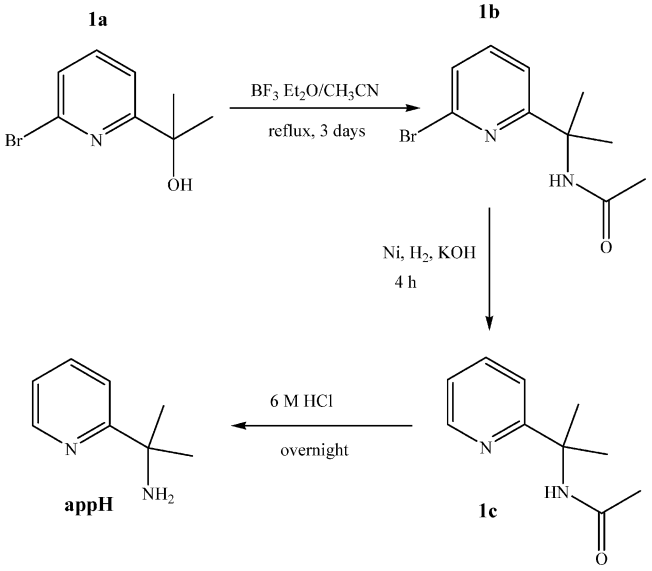

Scheme 4. General Preparation of the Complexes *trans*-RuHCl(diphosphine)(diamine)

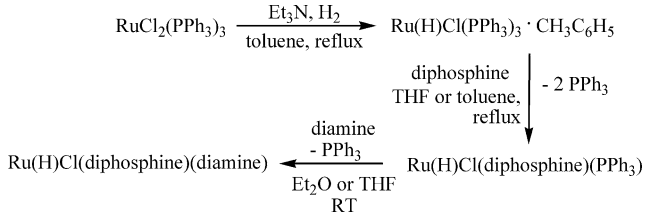

Et_2O for 72 h gives the amide **1b** in about 30% yield.[38] The bromo group can be easily removed with Raney Ni/H_2 under strongly basic conditions[39] to produce *N*-(2-(pyridin-2-yl)propan-2-yl)acetamide (**1c**) in about 65% yield. An acid-catalyzed hydrolysis of **1c** yields the new compound appH in good yield (>90%).

Any attempt to increase the yield of **1b** by changing the CH_3CN:BF_3Et_2O ratio or prolonging the reflux did not result in an increase in yield. The bromo substituent in the starting alcohol seems to be necessary because 2-(pyridin-2-yl)propan-2-ol does not react under similar conditions. The reason for this difference in the reactivity is not clear at the moment. The efforts to shorten the synthetic route by converting the alcohol to azide, which could be subsequently reduced to the pyridyl-amine, failed. The usual conversion of tertiary alcohols to azides using NaN_3 in acidic media did not produce the intermediate azide. The lack of reactivity could be due to the acid protonating the pyridyl nitrogen instead of converting the −OH group to the good leaving group H_2O.

Syntheses of Ru(II) Complexes. The ruthenium(II) chlorohydrido compounds of the general formula RuHCl(diphosphine)(diamine) have proven to be valuable precursors to the catalytically active amido and dihydride complexes.[7,13,33] These can be prepared following the general and well-established route in Scheme 4.[40]

This approach requires the preparation and isolation of the two intermediates $Ru(H)Cl(PPh_3)_3$ and Ru(H)Cl(diphosphine)(PPh_3) before the final product is obtained by substitution of the last PPh_3 ligand with a desired diamine. As such, it can be time-consuming and the isolation of the intermediates is usually accompanied by losses of material. We looked for a new, simpler route to prepare the Ru(H)Cl(diphosphine)(diamine) precursors in order to shorten the preparation time and increase the overall yields.

Scheme 5. Preparation of the Complex Ru(H)Cl(*S*-binap)(appH) (2) from $RuCl_2$(*S*-binap)(PPh_3)

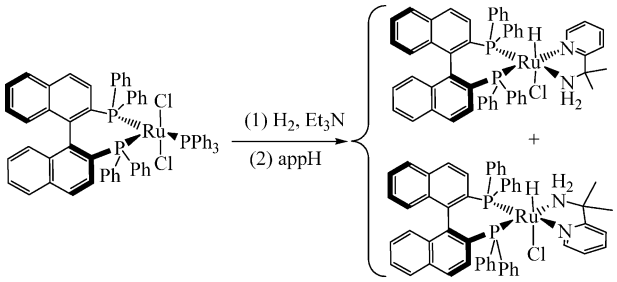

The chlorohydrido complex Ru(H)Cl(*S*-binap)(appH) (**2**) can be prepared in a two-step, one-pot reaction starting from $RuCl_2$(*S*-binap)(PPh_3)[41] (Scheme 5). In the first step, the starting dichloro complex is reacted with hydrogen gas under basic conditions to produce a deep red solution of the triphenylphosphine complex Ru(H)Cl(*S*-binap)(PPh_3) and the salt [Et_3NH]Cl as a precipitate. This reaction presumably proceeds via a dihydrogen intermediate, $RuCl_2(\eta^2\text{-}H_2)$(*S*-binap)($PPh_3$), in which the dihydrogen ligand is acidic enough to be deprotonated by the base NEt_3, as proposed in the formation of $Ru(H)Cl(PPh_3)_3$ from $RuCl_2(PPh_3)_3$ under analogous conditions.[42] The triphenylphosphine complex is not isolated from this reaction, but rather is reacted with appH to produce Ru(H)Cl(*S*-binap)(appH) (**2**). Complex **2** can be isolated as an orange-yellow solid.

Complex **2** exists as two diastereomers in approximately a 9:1 ratio on the basis of the integration in the ^{31}P NMR and ^1H spectra. The hydride-decoupled ^{31}P NMR spectrum has two sets of resonances in an AB pattern consistent with the presence of the two isomers. The hydride region of the ^1H NMR spectrum has two doublets of doublets at −15.8 and −16.3 ppm for the major and minor diastereomer, respectively. The magnitude of the $^2J_{HP}$ coupling constants is consistent with a hydride ligand cis to the P donor atoms of the *S*-binap on ruthenium. The proton resonances of the two methyl groups of each diastereomer appear as sharp singlets, consistent with the different environments syn to chloride and syn to hydride. Two broad doublets at 2.7 and 3.4 ($^2J_{HH}$ = 9.6 Hz) are assigned to inequivalent NH_2 protons; apparently these are coincident for the two diastereomers.

Complex **2** rapidly reacts with KO^{t}Bu under an argon atmosphere, eliminating an equivalent of HCl, to produce the deep red hydridoamido complex Ru(H)(*S*-binap)(app) (**3**) (Scheme 6). A sharp doublet of doublets in the hydride region of the ^1H NMR spectrum at −15.5 ppm and the magnitude of $^2J_{HP}$ coupling constants (26.1 and 40 Hz) indicate that the hydride ligand remains approximately cis with respect to two inequivalent phosphorus nuclei. Two CH_3 groups appear as two sharp singlets at 1.33 and 1.58 ppm, exhibiting a slight upfield shift compared to their resonances in **2.** A doublet at 4.3 ppm is assigned to the NH resonance with a $^3J_{HP}$ = 4.3 Hz due to the

(38) Sjöberg, K. *Acta Chem. Scand.* **1968**, *22*, 1787−1790.
(39) Kammerer, H.; Horner, L.; Beck, H. *Chem. Ber.* **1958**, *91*, 1376−1379.
(40) Abdur-Rashid, K.; Lough, A. J.; Morris, R. H. *Organometallics* **2001**, *20*, 1047−1049.
(41) Joshi, A. M.; Thorburn, I. S.; Rettig, S. J.; James, B. R. *Inorg. Chim. Acta* **1992**, *198*−*200*, 283−296.
(42) Jessop, P. G.; Morris, R. H. *Coord. Chem. Rev.* **1992**, *121*, 155−284.

Scheme 6. Preparation of the Hydridoamido Complex Ru(H)(*S*-binap)(app)

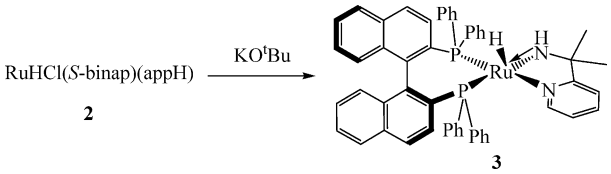

Table 1. Selected Bond Lengths (Å) and Angles (deg) for 3

bond (Å)		angle (deg)	
Ru1−H1ru	1.48(4)	P2−Ru1−H1ru	84(2)
Ru1−N1	1.962(3)	N1−Ru1−H1ru	127(2)
Ru1−N2	2.122(3)	N2−Ru1−H1ru	74(2)
Ru1−P1	2.234(1)	P1−Ru1−H1ru	106(2)
Ru1−P2	2.230(1)	P2−Ru1−N1	145.2(1)
		P1−Ru1−N2	168.69(9)
		N1−Ru1−N2	77.2(1)
		N2−Ru1−P2	100.23(9)
		P1−Ru1−P2	90.97(4)
		N1−Ru1−P1	94.5(1)

coupling to a phosphorus trans to the amido nitrogen. This assignment is based on the integration and on a ^{1}H 2D COSY experiment in which this resonance did not show coupling to any other proton in the complex. The ^{31}P{^{1}H} NMR spectrum has two doublets for two inequivalent phosphorus atoms (71 and 82.7 ppm, $^2J_{PP}$ = 31 Hz). This is similar to that of the spectrum of the complex RuH(*R*-binap)(NHCMe$_2$CMe$_2$NH$_2$).[7]

As mentioned in the Introduction, amidohydrido complexes are proposed to be within the catalytic cycle for the asymmetric hydrogenation of polar bonds catalyzed by ruthenium binap complexes[7,12−14] but have not been structurally characterized. The X-ray crystal structure of **3** (Figure 1 and Table 1) reveals a five-coordinate, distorted trigonal-bipyramidal geometry at Ru, with the P1 and pyridyl nitrogen (N2) approximately trans to each other (P1−Ru1−N2 = 168.69(9)°) and occupying the apical positions. The amido nitrogen (N1)−ruthenium distance is 1.962(3) Å, which is comparable to the 1.967(1) Å bond length in the similar amido complex Ru(H)(PPh$_3$)$_2$(HNCMe$_2$-CMe$_2$NH$_2$),[13] but significantly shorter than the N(amino)−Ru distance of 2.163(2) Å in Ru(H)Cl(PPh$_3$)$_2$(ampy).[32] The other hydrido amido complex, RuH(PPh$_2$C$_6$H$_4$CH$_2$NCMe$_2$CMe$_2$-NHCH$_2$C$_6$H$_4$PPh$_2$), has an amido nitrogen−Ru distance of 2.001(2) Å.[43] The sum of angles around N1 (357.4°) is as expected for a planar, sp^2-hybridized nitrogen atom involved in pπ(N)→dπ(Ru) dative bonding. There is a small H−Ru−P2 angle of 83.7(1)° for these σ donors across from the amido nitrogen as observed for similar five-coordinate RuHXL$_3$, RhH$_2$-XL$_2$, and IrH$_2$XL$_2$ complexes.[13,44]

Preliminary work shows that RuCl$_2$(app)(*R*-binap) can be prepared in 78% yield from RuCl$_2$(PPh$_3$)(*R*-binap) by stirring in toluene for 16 h (^{31}P NMR (C$_6$D$_6$) 44.2 (d), 47.6 (d)) and identified by a single-crystal structure determination of poor quality.

Catalytic Activity. In the presence of a strong base such as KO^{t}Bu, complex **2** acts as a precatalyst for the H$_2$-hydrogenation of acetophenone in benzene under mild reaction conditions. The complete conversion of acetophenone to 1-phenylethanol is achieved in less than 1.5 h with the substrate:catalyst:KO^{t}Bu ratio of 300:1:25 under 10 atm of H$_2$ and room temperature. The alcohol is produced in 27% ee for *R*-1-phenylethanol. The

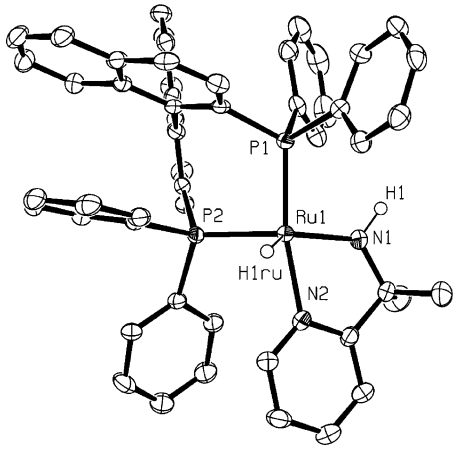

Figure 1. Structure of **3** with thermal ellipsoids shown at 50% probability. All the hydrogen atoms except the hydride and the amido NH are omitted for clarity.

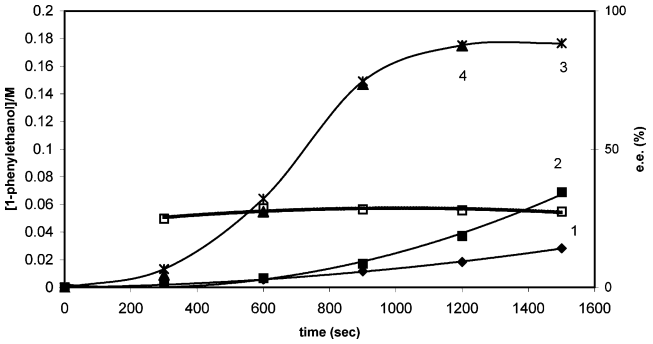

Figure 2. Kinetic data for hydrogenation of acetophenone catalyzed by **3** at 20 °C in C$_6$H$_6$: [**3**] = 0.0003 M, [acetophenone] = 0.3 M; constant pressure of 5 atm H$_2$ (run 1, ◆); [**3**] = 0.0003 M, [acetophenone] = 0.18 M, 5 atm H$_2$ (run 2, ■, corresponding ee values □); [**3**] = 0.0006 M, [acetophenone] = 0.18 M, 5 atm H$_2$ (run 3, *); and [**3**] = 0.0003 M, [acetophenone] = 0.18 M, 10 atm H$_2$ (run 4, ▲).

related complex Ru(H)Cl(ampy)(PPh$_3$)$_2$ (ampy = 2-aminomethylpyridine) gives 98% conversion after 1.3 h at room temperature using S:C:B ratio 709:1:17 and 5 atm H$_2$.[32] The amido complex **3**, on the other hand, is an active catalyst under base-free conditions. Using the same S:C ratio of 300:1, the complete hydrogenation of acetophenone to 1-phenylethanol was accomplished within the same reaction time.

The ketone 1-acetonaphthone was also tested since this more stereoactive substrate is often hydrogenated to the alcohol in high ee.[31,45,46] The amido complex **3** efficiently hydrogenates this substrate but only in 23% ee (*R*).

Kinetic Study. Several kinetic runs were performed using **3** as the catalyst and benzene as the solvent at constant hydrogen pressure (Figure 2). The behavior of this system, at low ketone conversions, is qualitatively similar to that previously reported for the amido complex Ru(H)(HNCMe$_2$CMe$_2$NH$_2$)(PPh$_3$)$_2$[13] and the dihydrides Ru(H)$_2$(*R*-binap)(tmen)[13] and Ru(H)$_2$(*R*,*R*-dach)-(PPh$_3$)$_2$[33] (tmen = 2,3-diamino-2,3-dimethylbutane; *R*,*R*-dach = (1*R*,2*R*)-1,2-diaminocyclohexane). The rate of alcohol production increases with an increase of either the catalyst concentration (run 2 vs run 3) or the dihydrogen concentration (run 2 vs run 4). On the other hand, the initial rate is not

(43) Li, T.; Churlaud, R.; Lough, A. J.; Abdur-Rashid, K.; Morris, R. H. *Organometallics* **2004**, *23*, 6239−6247.
(44) Riehl, J. F.; Jean, Y.; Eisenstein, O.; Pelissier, M. *Organometallics* **1992**, *11*, 729−737.
(45) Ralph, C. K.; Akotsi, O. M.; Bergens, S. H. *Organometallics* **2004**, *23*, 1484−1486.
(46) Chai, L. T.; Wang, W. W.; Wang, Q. R.; Tao, F. G. *J. Mol. Catal. A* **2007**, *270*, 83−88.

Scheme 7. Proposed Simple Mechanism (see below for a more complete mechanism) for the Hydrogenation of Acetophenone Catalyzed by 3 in Benzene with Low Concentrations of Alcohol (Path A) and High Concentrations of Alcohol (Path B)

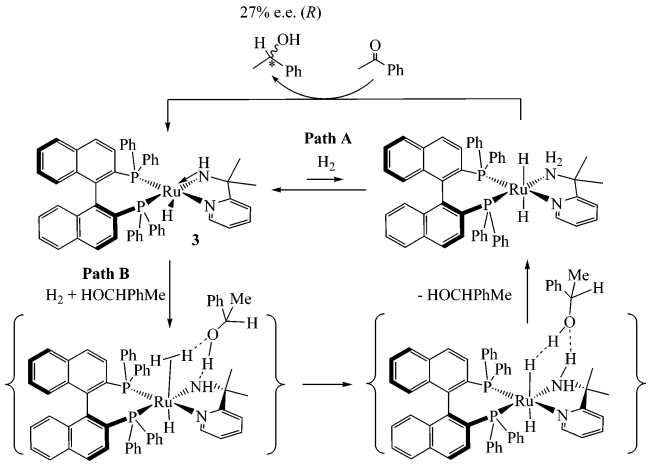

dependent on the substrate concentration (run 1 vs run 2). It is not clear for this complex, nonlinear reaction system why, later in the reaction, the higher ketone concentration (run 1) leads to a lower rate. However, overall these observations indicate that the heterolytic splitting of dihydrogen is the rate-determining step.

These observations on experiments at low ketone conversions and therefore low alcohol concentrations suggest the sequence of events as shown in path A of Scheme 7. The amido complex **3** heterolytically cleaves the H_2 molecule into a hydride on the metal and a proton on the amido nitrogen. The trans dihydride complex thus formed is responsible for the addition of $H^{(-)}/H^{(+)}$ to the C═O bond of the substrate to give 1-phenethanol in about 27% ee (*R*). Interestingly a solution of complex **3** in benzene-d_6, unlike the previous hydridoamido complexes,[13,47] does not react with 1 atm dihydrogen on the NMR scale (35 mg of complex in 0.55 mL of benzene-d_6 and 1 atm of H_2). Therefore the equilibrium constant for H_2 addition according to path A lies far to the left.

While the kinetic experiments with the dihydride catalysts $Ru(H)_2$(*R*-binap)(tmen) and $Ru(H)_2$(*R*,*R*-dach)$(PPh_3)_2$ show a linear production of alcohol over time, the systems with the RuH(*S*-binap)(app) catalyst show a significant acceleration in the rate as the reaction progresses. This suggests that the actual mechanism is more complicated than the one shown by path A of Scheme 7. The likely explanation for this observation is a lowering of the energy barrier for the dihydrogen splitting due to the assistance of the alcohol product. The alcohol might assist in the dihydrogen splitting via a six-membered transition state shown in path B of Scheme 7. In this scenario the alcohol protonates an amido nitrogen while the H_2 molecule is heterolytically cleaved between a Ru(II) center and an oxygen atom of the alkoxide. It is likely that this protonation−cleavage process occurs simultaneously through a hydrogen-bonded network.

Several other groups have suggested a similar alcohol-assisted mechanism in metal−ligand bifunctional catalysis. Ikariya and co-workers proposed, and also confirmed by use of isotope labeling experiments, that an alcohol-assisted dihydrogen splitting transition state accounts for the finding that the alcohols

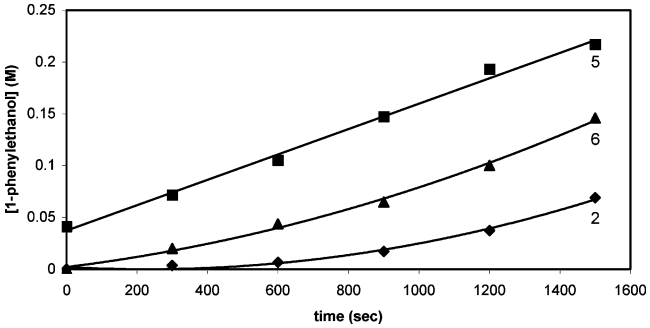

Figure 3. Data for the catalytic hydrogenation of acetophenone (0.18 M) in C_6H_6 at 20 °C with [**3**] = 0.0003 M under 5 atm of H_2 and no additive (run 2, ◆), *rac*-1-phenylethanol added (0.04 M, initial concentration) (run 5, ■), and 2-propanol added (0.06 M) (run 6, ▲).

such as 2-propanol and ethanol are the solvents of choice for the hydrogenation of arylketones catalyzed by some amine-hydrido ruthenium complexes.[48] In their kinetic study of the hydrogenation of acetophenone in 2-propanol using RuH(η^1-BH_4)(*S*-tolbinap)(1*S*,2*S*-dpen) (1*S*,2*S*-dpen = 1*S*,2*S*-diphenylethylenediamine) as a precatalyst, Noyori and co-workers suggested a transition state similar to that of path B for the regeneration of the active catalyst.[14] More recently, Casey and co-workers have established that there is ethanol-assisted loss of the H_2 molecule from Shvo's hydroxycyclopentadienyl ruthenium catalyst.[49]

The data of Figure 2 show that a critical concentration of the product has to build up in order for the rate to show a significant increase. This critical concentration can be estimated from the plots to be 9 mM for run 2 and 20 mM for runs 3 and 4 of Figure 2. Therefore this product concentration seems to be a function of both the catalyst concentration and H_2 pressure, and it roughly doubles by doubling either [Ru] or [H_2]. This also points to the alcohol's involvement in the reaction between the amido complex **3** and dissolved H_2. As more alcohol is produced during the reduction of the substrate, the participation of the alcohol in the H_2 splitting becomes more important and this produces an autocatalytic effect.

If 0.04 M racemic 1-phenylethanol is added at the beginning of the reaction, the resulting initial rate is significantly higher (Figure 3, Table 2). Additionally, the production of 1-phenylethanol remains almost linear until 100% conversion. If 2-propanol is added instead of *rac*-1-phenylethanol, the rate increases again but not as much as with the reaction product as an additive. The reason for the different effect on the rate of two alcohols may be the difference in acidity of the alcohols, the latter more acidic than the former. Since the proposed alcohol-assisted splitting of the H_2 molecule likely involves a simultaneous protonation of the amido nitrogen and reprotonation of the alcohol by the η^2-H_2 ligand, it is reasonable to expect that the acidity of the alcohol would be important. This is supported by the calculations described below.

The highest rate for the H_2-hydrogenation of acetophenone using **3** as a catalyst is observed in 2-propanol (run 7, Table 2). If benzene as a solvent is replaced with 2-propanol and other conditions are kept the same as in run 2, 95% conversion of the substrate to alcohol is achieved in only 5 min. This converts to a TOF of over 6750 h^{-1} in 2-propanol (run 7) compared to the final TOF of about 550 h^{-1} in benzene (run 2), calculated

(47) Rautenstrauch, V.; Hoang-Cong, X.; Churlaud, R.; Abdur-Rashid, K.; Morris, R. H. *Chem.−Eur. J.* **2003**, *9*, 4954−4967.

(48) Ito, M.; Hirakawa, M.; Murata, K.; Ikariya, T. *Organometallics* **2001**, *20*, 379−381.

(49) Casey, C. P.; Johnson, J. B.; Singer, S. W.; Cui, Q. *J. Am. Chem. Soc.* **2005**, *127*, 3100−3109.

Table 2. Turnover Frequencies, tof, for the Reduction of Acetophenone with 3 as a Catalyst (In all runs: [3] = 0.0003 M, [acetophenone] = 0.18 M, 5 atm H_2, 20 °C; runs 1−4 are shown in Figure 2)

run	solvent	additive	H or T?[a]	TOF, h^{-1} [b]	ee, % (*R*)
1−4	benzene	none	H	550	25−27
5	benzene	*rac*-$C_6H_5CH(OH)CH_3$ (0.04 M)	H	1520	
6	benzene	2-propanol (0.06 M)	H	1150	29
7	2-propanol	none	H	6750	32
8	2-propanol	none	T	115	37

[a] H = H_2 hydrogenation; T = transfer hydrogenation. [b] Values calculated on the basis of the conversion for the last point of each run.

Chart 1

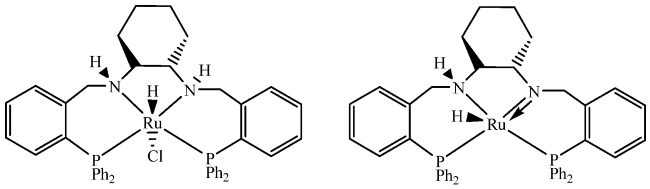

C **D**

for the last point of run 2. Under comparable solvent transfer hydrogenation conditions, that is, under Ar instead of H_2 gas, a conversion of only 12% was measured after 40 min. This gives a TOF of about 115 h^{-1} (Table 2, run 8).

There is a similar 10-fold increase in the catalysis rate constant on going from benzene to 2-propanol as the solvent for the precatalyst $RuHCl(PPh_2C_6H_4CH_2NHC_6H_{10}NHCH_2C_6H_4PPh_2)$ (complex **C**, Chart 1) containing a tetradentate P−NH−NH−P ligand.[47] The kinetic study with this catalyst revealed that in either benzene or 2-propanol the addition of the H_2 across the Ru−N amido bond of the complex **D** is the turnover-limiting step in the catalytic cycle.

The ee of the 1-phenylethanol for runs 1−6 (Figure 2, Table 2) ranges from 25 to 27% (*R* alcohol). A small increase to 32% was observed for the H_2-hydrogenation in 2-propanol (run 7) and further to 37% in transfer hydrogenation (run 8). These are somewhat higher than the ee value of 14% observed by Noyori for the hydrogenation of acetophenone catalyzed by the system $RuCl_2$(*S*-tolbinap)(ampy)/ base[34] using 2-propanol as a solvent. We find that $RuCl_2$(*R*-binap)(app) (note the use of *R*-binap here) when activated with KO^{t}Bu in 2-propanol displays a TOF of about 50 h^{-1} under the conditions listed in Table 2 to produce the *S* alcohol in 34% ee. Therefore the presence of the methyl groups of the appH ligand accounts for the difference in ee between the ampy and appH systems.

DFT Calculations. Theoretical studies have proven to be a useful tool in elucidating the mechanistic aspects of the catalytic hydrogenation of the polar, unsaturated bonds. Noyori and coworkers used this approach to support their metal−ligand bifunctional catalysis mechanism for transfer hydrogenation of ketones.[22] Some of us have used the results of DFT calculations as a support for the mechanism of H_2-hydrogenation of ketones established on the basis of kinetic data.[13] Hedberg et al. have extended these calculations to explain the alcohol effect on Noyori-type catalysts.[50] Other substrates have also been examined. For example, the hydrogenation of CO_2 using *cis*-$Ru(H)_2(PMe_3)_4$ catalysts has been a subject of a theoretical investigation.[51]

We extended our experimental results with a theoretical study in order to gain more information on the catalytic cycles shown in Scheme 7. Our choice of the restricted mPW1PW91[52,53] functional and the SDD[54] effective core potentials (ECP) for ruthenium is based on the previous reports showing that this combination is superior to the B3LYP functional and other ECP.[55,56] Recently, Lynch et al. have demonstrated that the mPW1PW91 functional is also better for the prediction of the transition states and the energy barriers.[57] All other nonmetallic elements were treated with the 6-311++G(d, p) level of theory.

For the gas-phase DFT calculations, catalyst **3** has been replaced with the model amido system $Ru(H)(PH_3)_2(2\text{-}NHCH_2(C_5H_4N))$ (**4**), in which the app$^-$ ligand has been replaced with a deprotonated ampy ligand, and *S*-binap, with the two PH_3 ligands. The optimized geometry of **4** (Figure 4) is quite similar to that of **3**. The $(HNCH_2C_5H_4N)^-$ ligand is almost planar, with the bridging $-CH_2-$ group displaced from the ligand plane. The length of the Ru−N(amido) bond in **4** is calculated to be 1.972 Å, and this compares very well with the corresponding distance of 1.962(3) Å in **3**. The geometry at the amido nitrogen in the model is trigonal planar, with the sum of the angles around nitrogen of 357.3° (compared with 357.4° in **3**). The Ru−N(pyridine) distance in **4** is 2.116 Å, while the corresponding one in **3** is 2.122(3) Å. The calculated Ru−H distance is somewhat longer than that in **3** from the X-ray study: 1.573 and 1.48(4) Å for **4** and **3**, respectively. However, this difference is likely to be the result of the fact that the X-ray diffraction method generally underestimates the metal−hydride distance. The bond angles are reproduced with less precision than the bond lengths. Thus, the hydride ligand is shifted toward the PH_3 trans to the amido nitrogen, much like in **3**, but the P−Ru−H angle in **4** (81.7°) is smaller than the corresponding one in **3** (83.7(2)°). On the other hand the P2−Ru−N1 angle is larger in **4** than in **3** (154.6° vs 145.2(1)°). However, in the last case the difference can be a consequence of replacing a rigid, bidentate ligand (*S*-binap) with the two much smaller monodentate PH_3 ligands. The discrepancy between the bond angles in a real complex and its model has been reported previously for various DFT functionals and basis sets.[56]

Mechanism for Low Concentrations of Alcohol, Path A. The theoretical reaction coordinate diagram for the H_2 activation and the subsequent acetone hydrogenation in the gas phase without alcohol assistance is shown in Figure 5. The structures corresponding to the steps of dihydrogen activation are shown in Figure 4, while those of acetone hydrogenation are shown in Figure 6. The profile of Figure 5 supports the experimental findings corresponding to low conversions (path A of Scheme 7) that the reaction between the amido catalyst and H_2 gas to produce *trans*,*cis*-$Ru(H)_2(PH_3)_2$(ampy) (**5**) via transition state

(50) Hedberg, C.; Källstrom, K.; Arvidsson, P. I.; Andersson, P. G.; Brandt, P. *J. Am. Chem. Soc.* **2005**, *127*, 15083−15090.
(51) Ohnishi, Y.; Matsunaga, T.; Nakao, Y.; Sato, H.; Sakaki, S. *J. Am. Chem. Soc.* **2005**, *127*, 4021−4032.
(52) Adamo, C.; Barone, V. *J. Chem. Phys.* **1998**, *108*, 664−675.
(53) Burke, K.; Perdew, J. P.; Wang, Y. In *Electronic Density Functional Theory: Recent Progress and New Directions*; Dobson, J. F., Vignale, G., Das, M. P., Eds.; Plenum: New York, 1997; p 81.
(54) Leininger, T.; Nicklass, A.; Stoll, H.; Dolg, M.; Schwerdtfeger, P. *J. Chem. Phys.* **1996**, *105*, 1052−1059.
(55) Gusev, D. G. *J. Am. Chem. Soc.* **2004**, *126*, 14249−14257.
(56) Zhang, Y.; Guo, Z.; You, X.-Z. *J. Am. Chem. Soc.* **2001**, *123*, 9378−9387.
(57) Lynch, B. J.; Truhlar, D. G. *J. Phys. Chem. A* **2001**, *105*, 2936−2941.

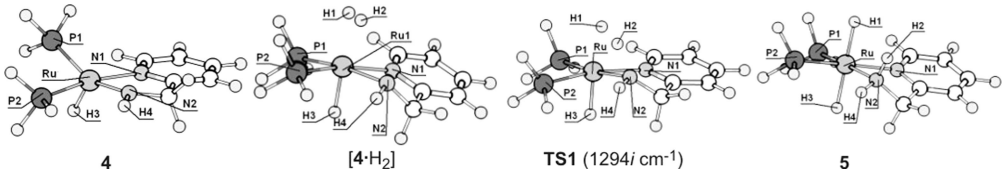

Figure 4. Optimized gas-phase structures of the model complexes and the transition state (**TS1**) for the dihydrogen splitting without an alcohol. Selected bond lengths and angles: **4** Ru−N1 2.116 Å, Ru−N2 1.971 Å, Ru−H3 1.573 Å, Ru−N2−H4 126.5°; [**4**·H_2] Ru−N2 2.103 Å, H1−H2 0.812 Å, Ru−H1 1.845 Å, Ru−H2 1.832 Å, Ru−H3 1.601 Å, Ru−N2−H4 107.5°, **TS1** Ru−N2 2.153 Å, H1−H2 1.029 Å, Ru−H1 1.809 Å, N2−H2 1.832 Å, Ru−H3 1.634 Å, Ru−N2−H4 108.2°, **5** Ru−N2 2.166 Å, H1−H2 2.6 Å, Ru−H1 1.681 Å, Ru−H3 1.703 Å, Ru−N2−H4 105.6°. Selected APT charges of [**4**·H_2]: H_1 +0.095, H_2 +0.091, N_2 −0.48.

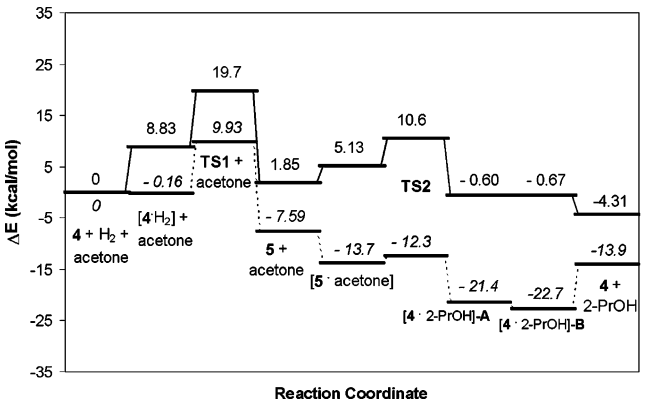

Figure 5. Calculated energies (at the mPW1PW91/SDD level for Ru and mPW1PW91/6-311++G(d,p) level for the nonmetallic elements) for the H_2-hydrogenation catalytic cycle using **4** as a model catalyst and acetone as a substrate (ΔH dashed line, ΔG solid line). The ΔG values (298.15 K, 1 atm) are corrected for the zero-point energies but uncorrected for translation and rotation.

TS1 is the turnover-limiting step with theoretical (gas-phase) activation energies of 19.7 ($\Delta G^{\ddagger}$) and 9.9 kcal/mol ($\Delta H^{\ddagger}$), respectively. The energies of hydrogenation of acetone are calculated to be −4.31 (ΔG) and −13.9 kcal mol^{-1} (ΔH), respectively.

The dihydrogen activation steps (Figures 4 and 5) start with the **4**/H_2 system consisting of free **4** and free H_2. When H_2 is placed above the plane defined by Ru and two N atoms (at approximately 3.5 Å distance) and the system is optimized, the dihydrogen complex [**4**·H_2] is obtained (Figure 4). This complex is the dihydrogen-hydride species Ru(η^2-H_2)(H)(PH_3)$_2$-($HNCH_2C_5H_4N$). The H−H distance in [**4**·H_2] (0.812 Å) is longer than the H−H distance in free H_2 (0.744 Å). The APT charges on the H atoms (+0.095 and +0.091) indicate that the coordinated H_2 molecule becomes acidic.[42] The H_2 ligand is oriented in such a way that it eclipses the Ru−N(amido) bond. If it is rotated to eclipse the Ru−N(pyridine) bond and reoptimized, the H_2 returns to eclipse the Ru−N(amido) during the optimization steps. The higher stability of the former structure stems from the higher electron density around the formally double Ru−N(amido) bond that could contribute to back-bonding to σ^* (H_2). The consequence of the H_2 coordination is the loss of planarity at the N(amido) (sum of angles at N is 327.4°), its rehybridization from sp^2 to sp^3, and the resulting release of the nitrogen lone pair from $p\pi$(N)→$d\pi$(Ru) dative bonding. Consequently, the Ru−N(amido) bond elongates from 1.972 Å in **4** to 2.103 Å in [**4**·H_2] and the APT charge on nitrogen atom decreases from −0.454 to −0.479. reflecting its increased basicity.

The acidic η^2-H_2 ligand in [**4**·H_2] is deprotonated by the amido nitrogen to produce the trans dihydride *trans*,*cis*-Ru(H)$_2$(PH_3)$_2$-(ampy) (**5**) via the transition state **TS1** (Figure 4). The start of N−H and Ru−H bond formation in **TS1** is signaled, among other changes, by an elongation of the H−H distance (to 1.029 Å) and a shortening of the N···H and Ru···H distances to 1.832 and 1.809 Å, respectively. The imaginary frequency for this mode is 1294*i* cm^{-1}. The activation parameters for **TS1** ($\Delta G^{\ddagger}$ = 19.7 kcal mol^{-1}, $\Delta H^{\ddagger}$ = 9.93 kcal mol^{-1}, $\Delta S^{\ddagger}$ = −32.7 cal mol^{-1} K^{-1}) compare well with those experimentally determined for Ru(H)$_2$(*R*-binap)(tmen) ($\Delta G^{\ddagger}$ = 16.6 kcal mol^{-1}, $\Delta H^{\ddagger}$ = 8.6 kcal mol^{-1}, $\Delta S^{\ddagger}$ = −27 cal mol^{-1} K^{-1}) and Ru(H)-(PPh_3)$_2$($HNCMe_2CMe_2NH_2$) ($\Delta G^{\ddagger}$ = 14.5 kcal mol^{-1}, $\Delta H^{\ddagger}$ = 7.6 kcal mol^{-1}, $\Delta S^{\ddagger}$ = −23 cal mol^{-1} K^{-1}).[13]

The geometry at Ru in the trans dihydride **5** is that of a distorted octahedron. Overall, it closely resembles the geometry of a related trans dihydride Ru(H)$_2$(*R*-binap) ($H_2NCMe_2CMe_2$-NH_2), whose X-ray crystal structure has been determined.[7] The Ru−H distances in **5** are 1.681 and 1.703 Å, while those in Ru(H)$_2$(*R*-binap) ($H_2NCMe_2CMe_2NH_2$) are 1.64(3) and 1.70-(3) Å. The Ru−NH_2 bond lengths are also comparable with 2.166 Å in **5** and 2.202(2)/2.193(2) Å in the full complex. Interestingly, the P−Ru−P angle in **5** (91.4°) is almost identical

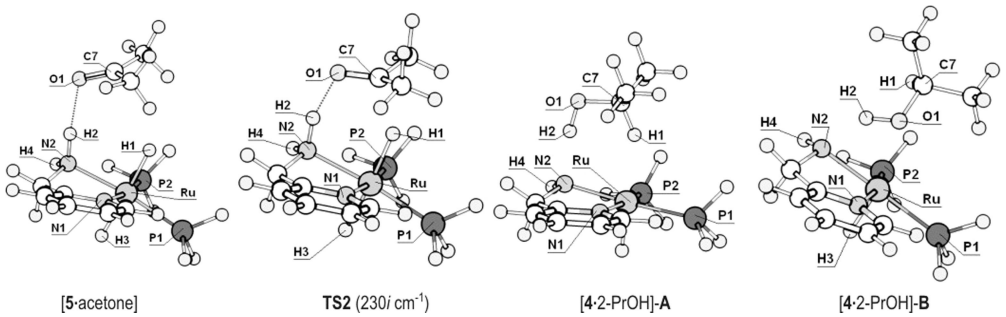

Figure 6. Optimized gas-phase structures of the model complexes and the transition state (**TS2**) for the H_2-hydrogenation of acetone with **5** as catalyst. Selected bond lengths (Å): [**5**·acetone] H1−C7 2.926, O1−C7 1.216, O1−H2 1.980, H2−N2 1.019, N2−Ru 2.165, Ru−H1 1.688, **TS2** H1−C7 1.817, O1−C7 1.241, O1−H2 1.725, H2−N2 1.035, N2−Ru 2.139, Ru−H1 1.724, [**4**·2-PrOH]-**A** H1−C7 1.127, O1−C7 1.419, O1−H2 1.004, N2−H2 1.698, Ru−N2 2.052, Ru−H1 2.181, [**4**·2-PrOH]-**B** H1−C7 1.100, O1−C7 1.419, O1−H2 1.006, N2−H2 1.715, Ru−N2 2.094, Ru−O1 2.380.

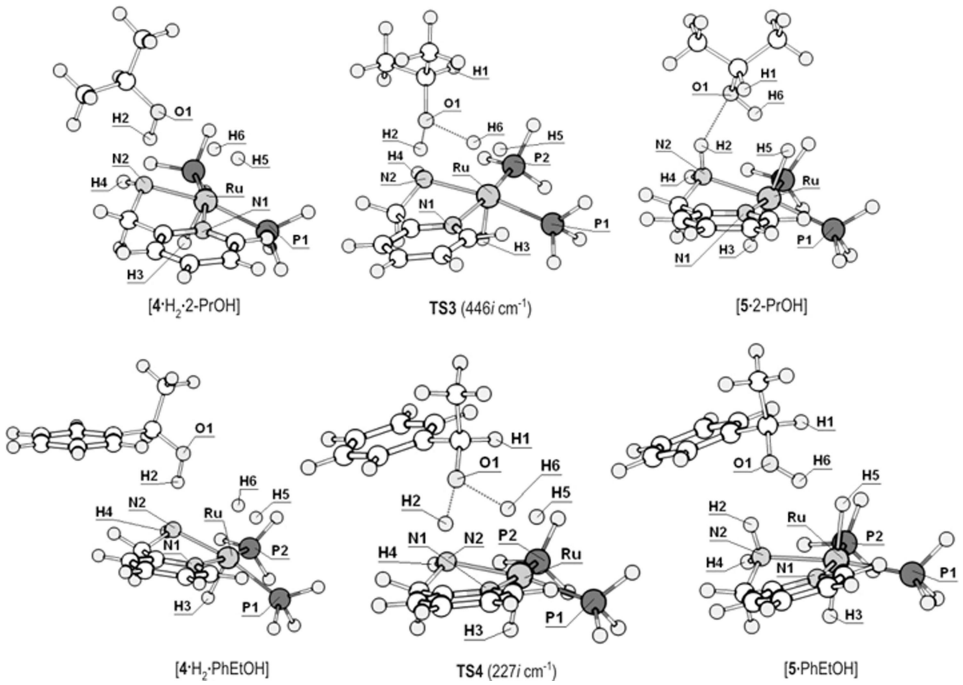

Figure 7. Optimized gas-phase structures of the model complexes and the transition states for the 2-propanol- and 1-phenylethanol-assisted splitting of H_2. Selected bond lengths (Å): [**4**·H_2·2-PrOH] H5−H6 0.813, Ru−H5 1.830, Ru−H6 1.849, O1−H6 2.434, H2−N2 1.708, **TS3** H5−H6 0.857, Ru−H5 1.817, O1−H6 1.648, H2−N2 1.154, [**5**·2-PrOH] H6−H5 1.648, Ru−H5 1.706, O1−H6 0.990, H2−N2 1.024, O1−H2 1.933, [**4**·H_2·PhEtOH] H5−H6 0.814, Ru−H5 1.831, Ru−H6 1.842, O1−H6 2.543, H2−N2 1.660, **TS4** H5−H6 0.851, Ru−H5 1.818, O1−H6 1.684 Å, H2−N2 1.120, [**5**·PhEtOH] H6−H5 1.487, Ru−H5 1.708, O1−H6 0.995, H2−N2 1.022, O1−H2 2.027. Selected APT charges of [**4**·H_2·2-PrOH]: H_5 +0.10, H_6 +0.14, N_2 −0.58; [**4**·H_2·PhEtOH]: H_5 +0.11, H_6 +0.12, N_2 −0.58.

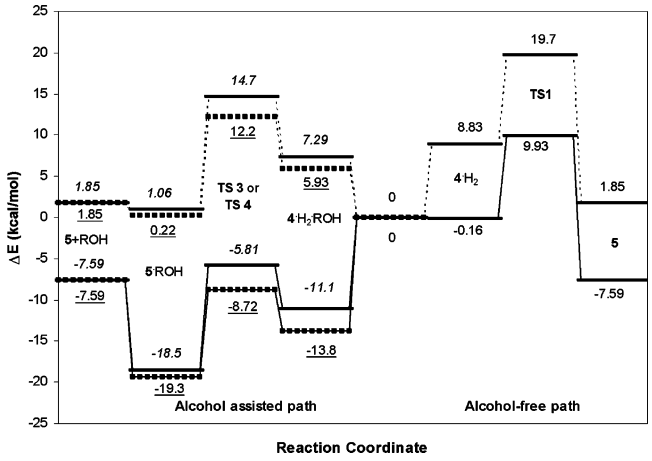

Figure 8. Comparison of the calculated energies for the alcohol-free H_2 splitting (from the middle to the right) and the alcohol-assisted H_2 splitting (from the middle to the left). The zero value at the middle is the starting relative energy of free **4** and H_2 for the alcohol-free path and free **4**, H_2, and alcohol for the alcohol-assisted path. The ΔG values (298.15 K, 1 atm) are corrected for the zero-point energies but uncorrected for translations and rotations. The solid line connects ΔH, while the dashed line connects ΔG values. The values for R = $C_6H_5(CH_3)CH-$ are underlined, while those for R = $(CH_3)_2CH-$ are in italics.

to the P−Ru−P angle in Ru(H)$_2$(*R*-binap)($H_2NCMe_2CMe_2NH_2$) (91.5°). The formation of **5** is entropically unfavorable, and **5** lies about 2 kcal/mol in free energy above free H_2 and **4**. This may be why the formation of the corresponding dihydride *trans*-Ru(H)$_2$(*S*-binap)(appH) from **3** and dihydrogen gas (1 atm) has not yet been observed.

Figure 5 also shows the energy profiles for the reaction of the trans dihydride **5** with acetone via transition state **TS2** to give back the hydridoamido complex **4** and release 2-propanol as a model of a ketone hydrogenation reaction. There are small barriers to this exothermic reaction. First the trans dihydride **5** interacts with acetone to produce the molecular complex [**5**·acetone] (Figure 6), where the carbonyl oxygen forms a hydrogen bond with the axial proton of the NH_2 group and the carbonyl carbon interacts weakly with the hydride on Ru. This interaction causes a slight elongation in the C═O bond from 1.207 Å in free acetone to 1.216 Å in [**5**·acetone].

The hydrogenation of acetone proceeds via a transition state **TS2** that has an imaginary frequency at 230*i* cm^{-1}. The transfer of $H^{(-)}$ and $H^{(+)}$ in an outer-sphere mechanism is facile with the activation parameters $\Delta G_{hyd}^{\ddagger}$ = 8.7 kcal mol^{-1}, $\Delta H_{hyd}^{\ddagger}$ = −4.7 kcal mol^{-1}, and $\Delta S_{hyd}^{\ddagger}$ = −76.6 cal mol^{-1} K^{-1}. In **TS2** there is a significant shortening of the C···H and O···H distances in the O═C···H−Ru and C═O···H−N interactions, respectively, and an elongation of the C−O bond. Other changes are also apparent during the vibration at the imaginary frequency. These include a significant displacement of the carbonyl carbon from the plane defined by the two methyl carbons and the oxygen atom and also a movement of the hydride ligand toward the electrophilic carbon in the C═O group.

The primary product of acetone hydrogenation is the adduct [**4**·2-PrOH]-**A**, in which 2-propanol interacts with the amido complex through N2···H2−O1 (1.70 Å) and C7−H1···Ru (2.18 Å) interactions (Figure 6). Complex [**4**·2-PrOH]-**A** can rearrange to produce [**4**·2-PrOH]-**B**, which is, according to calculations, the most stable structure of the cycle (Figure 5). 2-Propanol is still in close contact with the amido nitrogen (N2···H2−O1 distance 1.71 Å); however the Ru···H1 interaction is lost and rather the O1 atom from 2-propanol moves above the ruthenium atom (O1···Ru 2.38 Å). As a result, the Ru−N(amido) bond in [**4**·2-PrOH]-**B** is significantly longer than the same bond in free **4** (2.094 vs 1.972 Å). This indicates a decrease in the pπ(N)→dπ(Ru) dative bonding due to the fact that the nitrogen lone pair is involved in the interaction with the alcohol. Also,

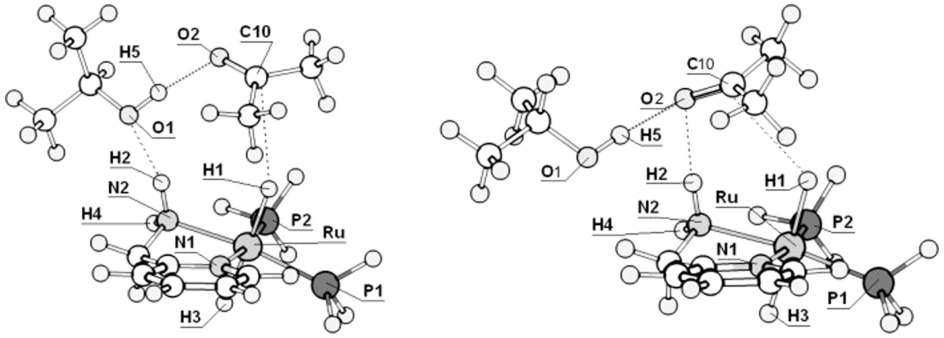

Figure 9. Optimized starting structures (gas phase) for the alcohol-assisted hydrogenation of acetone. Selected bond lengths (Å): **6** H1−C10 3.114, C10−O2 1.218, O2−H5 1.819, O1−H2 2.009, **7** H1−C10 2.973, C10−O2 1.221, O2−H2 2.145, O2−H5 1.902.

Scheme 8

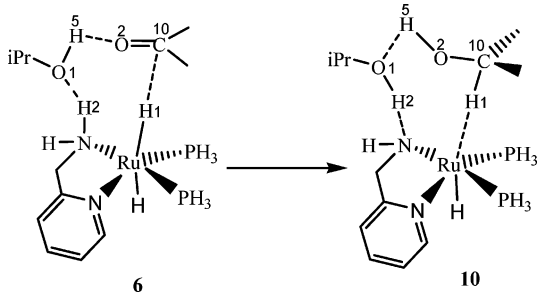

the geometry around the N(amido) is not trigonal planar (sum of angles at N is 334.6°). Its APT charge decreases from −0.474 in **4** to −0.540 in [**4**·2-PrOH]-**B**, indicative of higher localization of the negative charge. In this environment, the Ru center is more electron-deficient. After 2-propanol is released from [**4**·2-PrOH]-**B**, the active catalyst **4** is regenerated.

It is interesting to note that every attempt to obtain a stable structure [**5**·acetophenone], an analogue of [**5**·acetone], failed. The result of the optimization steps was the hydrogenation of the substrate and the formation of **4** and 1-phenylethanol, a structural analogue to [**4**·2-PrOH]-**A**. The same outcome was obtained regardless of the size of basis sets used for nonmetallic elements (3-21G(d,p) and 6-311++G(d,p)) and the distance between **5** and acetophenone molecules in the Gaussian input file. This result suggests that the energy barrier for the acetophenone hydrogenation is significantly lower than that for acetone and in turn lies even lower compared to the H_2 splitting step.

Alcohol-Assisted H_2 Splitting Mechanism, Path B. This mechanism (path B of Scheme 7), involving either 2-propanol or 1-phenylethanol, has also been investigated theoretically (Figures 7−9). The addition of the η^2-H_2 ligand to the electron-deficient and coordinatively unsaturated Ru center in [**4**·ROH]-**B** (R = $(CH_3)_2CH$− or $C_6H_5(CH_3)CH$−) produces stable η^2-dihydrogen complexes [**4**·H_2·ROH] (Figure 7). These consist of [**4**·H_2] (see above) in a hydrogen-bonded network with the respective alcohol. One H atom of the dihydrogen ligand is oriented toward the oxygen atom in the alcohol (as opposed to the amido nitrogen in [**4**·H_2]), while the N(amido)···HO hydrogen bond remains intact. The H−H distances in [**4**·H_2·ROH] are similar to that of [**4**·H_2], but the dihydrogen atoms in [**4**·H_2·ROH] have a positive charge (APT) (Figure 7) that is approximately 0.05 units greater than those of [**4**·H_2] (Figure 4). Furthermore, the amido nitrogen is more basic, with a negative charge of −0.58 for [**4**·H_2·ROH] compared to −0.48 for [**4**·H_2]. The dihydrogen is cleaved between the Ru and the oxygen atom via the transition states **TS3** and **TS4** (Figure 7), each with one imaginary frequency at 446*i* and 227*i* cm^{-1}. The splitting of the H_2 and the simultaneous protonation of the amido nitrogen are indicated by a decrease in HH···O and OH···N distances. After the heterolytic H_2 cleavage, the complexes [**5**·ROH] are produced in which the alcohol is hydrogen bonded to the trans dihydride complex **5**. Hedberg et al. calculated a very similar enthalpy profile for the $RuH(NHCH_2CH_2NH_2)(PH_3)_2/H_2$/MeOH system.[50]

The activation parameters for the alcohol-assisted transition states **TS3** for 2-PrOH ($\Delta G_a^{\ddagger} = 14.7$ kcal mol^{-1}, $\Delta H_a^{\ddagger} = -5.81$ kcal mol^{-1}, $\Delta S_a^{\ddagger} = -68.7$ cal mol^{-1} K^{-1}) and **TS4** for 1-phenylethanol ($\Delta G_a^{\ddagger} = 12.2$ kcal mol^{-1}, $\Delta H_a^{\ddagger} = -8.72$ kcal mol^{-1}, $\Delta S_a^{\ddagger} = -70.3$ cal mol^{-1} K^{-1}) lie significantly below the ones calculated for the alcohol-free **TS1** (Figure 8). The change in $\Delta G_a^{\ddagger}$ due to 2-propanol assistance is approximately −5 kcal/mol, and this should result, on the basis of gas-phase transition state theory, in an increase in the rate constant by a factor of 4000. In the actual experiment, a factor of about 10 is observed on going from benzene to 2-propanol. There must be other factors in solution compared to the gas phase that have not been considered, such as those arising from differences in the pre-exponential factor of the rate constant equation for the ternary transition state complex **TS3** versus the secondary transition state complex **TS1** or other interactions of the catalyst or transition states with further alcohol molecules. The factor of 10 increase in rate constant cannot be simply explained by a nonspecific polarity effect since the change in polarity during the hydrogenation of a 0.2 M ketone solution in benzene is negligible, yet a sizable increase in rate is observed.

Alcohol-Assisted Ketone Hydrogenation. Since Figure 8 indicates that the solvated dihydride complex [**5**·2-PrOH] would be favored over "free" **5** in 2-propanol solutions, we investigated how the ketone hydrogenation by this dihydride is affected by the presence of a 2-propanol molecule. Very recently Handgraaf and Meijer have utilized *ab initio* molecular dynamics methods to evaluate the role of the alcohol solvent in the transfer hydrogenation of formaldehyde to methanol using (η^6-C_6H_6)$RuH(NH_2CH_2CH_2O)$ as a catalyst.[58] They showed that the solvent molecules can play a specific role in the substrate reduction process and that simple solvation models cannot account for this.

We examined two possible starting points for the alcohol-assisted hydrogenation of acetone (H_2 transfer), systems **6** and **7** (Figure 9).

(58) Handgraaf, J.-W.; Meijer, E. J. *J. Am. Chem. Soc.* **2007**, *129*, 3099−3103.

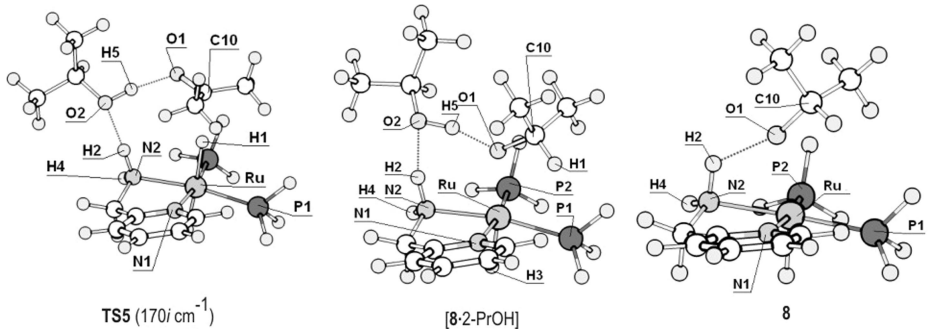

Figure 10. Optimized gas-phase structures of the model complexes and the transition state (**TS5**) for the alcohol-assisted ketone hydrogenation starting from **6**. Selected bond lengths (Å): **TS5** H1−C10 1.786, C10−O1 1.241, O1−H5 1.658, O2−H2 1.869, [**8**·2-PrOH] Ru−O1 2.206, O1−C10 1.388, O1−H5 1.513, O2−H2 1.779, **8** Ru−O1 2.182, O1−H2 1.825, O1−C10 1.379.

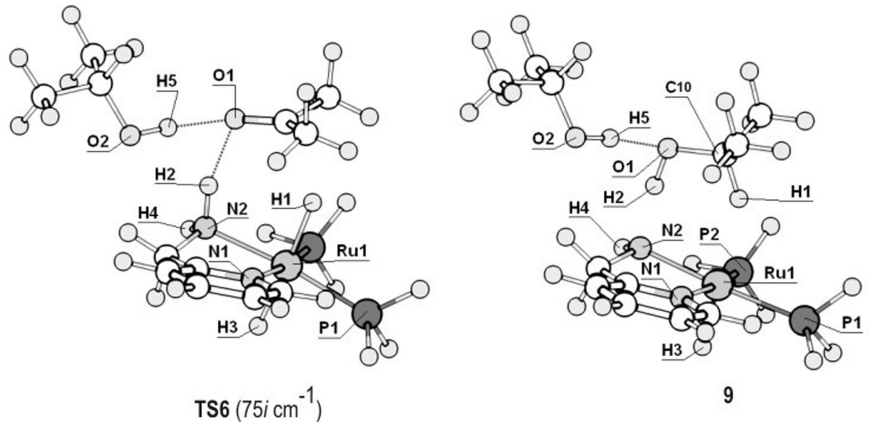

Figure 11. Optimized gas-phase structures of the model complexes and the transition state (**TS6**) for the alcohol-assisted ketone hydrogenation starting from **7**. Selected bond lengths (Å): **TS6** H1−C10 2.087, H2−O1 1.882, H5−O1 1.859, O1−C10 1.235, **9** H1−C10 1.125, O1−C10 1.400, O1−H2 1.033, H2−N2 1.581, H5−O1 1.811.

Structure **6** (Figure 9) results from insertion of the acetone carbonyl group into the OH···HRu hydridic-protonic bond of the complex [**5**·2-PrOH]. Thus an eight-membered ring is formed through a hydrogen bond network. Structure **7** is obtained by adding a 2-propanol molecule to [**5**·acetone] so that it forms a hydrogen bond to the carbonyl group of the acetone. This retains the original six-membered ring of the complex [**5**·acetone]. System **7** is slightly higher in energy than **6** ($\Delta H = 0.70$ kcal/mol, $\Delta G = 1.03$ kcal/mol), and thus the two could be in equilibrium.

Starting from complex **6**, we expected to complete the hydrogenation of acetone by "shuttling" the protons through the hydrogen bond network according to Scheme 8 to give complex **10**. However, our attempts to optimize the structure of complex **10** failed. Instead the calculations predict the formation of the alkoxohydridoruthenium(II) complex [**8**·2-PrOH] (Figure 10). This species is the product of only a hydride transfer to the carbonyl carbon.

These results suggest that the alcohol −OH group is not acidic enough to transfer its proton to the substrate. The proton on the neighboring $-NH_2$ group is tied up in a hydrogen bond with the alcohol molecule. The optimized structure of [**8**·2-PrOH] is very similar to the crystal structure of the related Ru(II) phenoxide complex RuH(OPh)(tmen)(PPh_3)·HOPh (tmen = 2,3-diamino-2,3-dimethylbutane),[26] in which a phenol molecule forms a six-membered ring Ru−O···HO(Ph)···NH with the pseudo-octahedral complex through a hydrogen bond network. However, the bonds in [**8**·2-PrOH] are much shorter than the corresponding ones in the phenoxide complex. Thus the Ru−O distance in the phenoxide complex is 2.364(2) Å, while the calculated one in [**8**·2-PrOH] is 2.206 Å and compares well with the Ru−O distance of 2.239(2) Å in a similar complex, *trans*-RuH(OC_6H_4-*p*-CH_3)(dmpe)$_2$ (dmpe = $Me_2PCH_2CH_2PMe_2$).[59] The calculated hydrogen bonds in [**8**·2-PrOH] are also shorter (OH···HRu 1.51 Å and NH···OH 1.78 Å) compared to the phenoxide/phenol complex (OH···HRu 1.72 Å and NH···OH 2.04 Å). This difference in hydrogen bonds could be the consequence of inaccuracy in hydrogen atom positions and bond lengths as determined by X-ray crystallography. The O(alcohol)−O(Ru alkoxide) (2.51 vs 2.52 Å in [**8**·2-PrOH] and phenoxide, respectively) and O(alcohol)−N(Ru) distances (2.80 vs 2.93 Å) are comparable. The transition state for the formation of [**8**·2-PrOH], **TS5**, has the activation parameters $\Delta G_a^{\ddagger} = 14.4$ kcal mol^{-1}, $\Delta H_a^{\ddagger} = -17.7$ kcal mol^{-1}, and $\Delta S_a^{\ddagger} = -107$ cal mol^{-1} K^{-1} (relative to the free reactants: amido **4**, acetone, H_2, and 2-propanol) with an imaginary frequency at 170*i* cm^{-1}. It is interesting to note that the calculated values for $\Delta G_a^{\ddagger}$ for **TS3** (2-propanol-assisted H_2 splitting) and **TS5** are very close: 14.7 and 14.4 kcal/mol. The loss of the 2-propanol molecule produces alkoxide complex **8**. Complex **8** is characterized by a short H2···O1 distance of 1.82 Å accompanied by a small N2−Ru−O1 angle of 71.6° (compared to 84.9° in [**8**·2-PrOH]) while maintaining the Ru−O1 bond almost unchanged at 2.182 Å. Bergens and co-workers[19] have recently reported the observation of RuH(2-PrO)(*R*-binap)(*R*,*R*-dpen) formed from [RuH(H_2)(*R*-binap)(*R*,*R*-dpen)]$^+$ in 2-propanol in the presence of a strong base (KO^{t}Bu). They have provided evidence that this alkoxide complex does not react with H_2 (2 atm) without a base present at ambient temperatures over prolonged times (10 h). The remarkable stability of the observed alkoxide was attributed to

(59) Burn, M. J.; Fickes, M. G.; Hollander, F. J.; Bergman, R. G. *Organometallics* **1995**, *14*, 137−150.

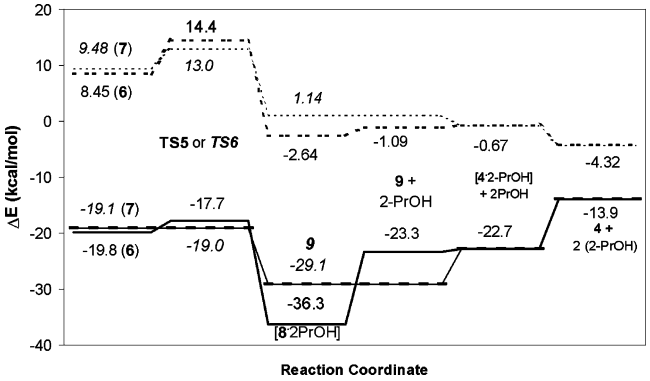

Figure 12. Part of the energy profile for the alcohol-assisted hydrogenation of acetone, starting from **6** or **7** (Figure 9). The solid lines connect the Δ*H*, while the dashed lines connect the Δ*G* values. The energy values for the cycle starting with **6** are in normal font, while those for the cycle starting from **7** are in italics. The energies are relative to free **4**, acetone, 2-propanol, and H_2 for easier comparison with the energy profiles of Figure 8. The reaction sequence ends with two free 2-propanol and the regenerated free amido **4**.

the intra- and/or intermolecular hydrogen bonding between an NH group and the 2-PrO$^-$ ligand and/or solvent molecules.[19] Our calculations support this observed stability. Given that the alkoxohydridoruthenium complexes are not active in the H_2-hydrogenation of ketones[26] and have high stability,[19] they possibly represent the catalyst resting state in 2-propanol solutions. The addition of a strong base presumably shifts the equilibrium toward the formation of free **4** and thus decreasing the concentration of the resting state species.[19] Experimental observations have shown that the addition of base has a beneficial effect on the rate of hydrogenation.[14,33] However, there is a small difference in free energy between **8** and complex [**4**·2-PrOH]-**B** (0.6 kcal/mol), suggesting that the two might be in a rapid equilibrium.

An alternative pathway starts from the hydrogen-bonded system **7** (Figure 9). In this case a structure **9** is found (Figure 11), in which the proton from the amino group and the hydride from the RuH moiety have been fully transferred to the ketone substrate. In **9** the hydrogen bond between 2-propanol and hydrogenated substrate (O(2)H(5)···O(1)) is retained and described as [**4**·2-PrOH]-**A** with one 2-propanol molecule hydrogen bonded to the newly produced alcohol. The transition state **TS6** has the activation parameters $\Delta G_a^{\ddagger} = 13.0$ kcal mol^{-1}, $\Delta H_a^{\ddagger} = -19.0$ kcal mol^{-1}, and $\Delta S_a^{\ddagger} = -107$ cal mol^{-1} K^{-1} (relative to the free reactants: amido **4**, acetone, H_2, and 2-propanol) with an imaginary frequency at 75*i* cm^{-1}. The energy profile of the two pathways is shown in Figure 12.

The transition states for alcohol-assisted hydrogen splitting (**TS3**) and alcohol-assisted H_2 transfer (**TS5** and **TS6**) are very close in free energy (14.7, 14.4, and 13.0 kcal/mol for **TS3**, **TS5**, and **TS6**, respectively), but in any case the H_2 splitting has a higher energy barrier. Furthermore, the orientation of the substrate molecule in **TS5** and **TS6** is different from that in **TS2** (alcohol-free hydrogenation). Since this is the step that determines enantioselectivity, this difference in orientation can explain the difference in obtained ee values between the reactions in benzene and 2-propanol (27 vs 32%; see Table 2). It might also explain the dramatic changes in ee with solvent reported by Ohkuma et al. with the very similar complex $RuCl_2$-((*S*)-tolbinap)(pica), where pica and ampy refer to the same ligand, 2-aminomethylpyridine.[34] Ohkuma et al. attributed the changes to variations in the structures of the alkoxides *cis*-RuH-(OR)((*S*)-tolbinap)(pica), which they propose to be the active

Scheme 9. Expanded Mechanism to Include Catalysis in Benzene and 2-PrOH

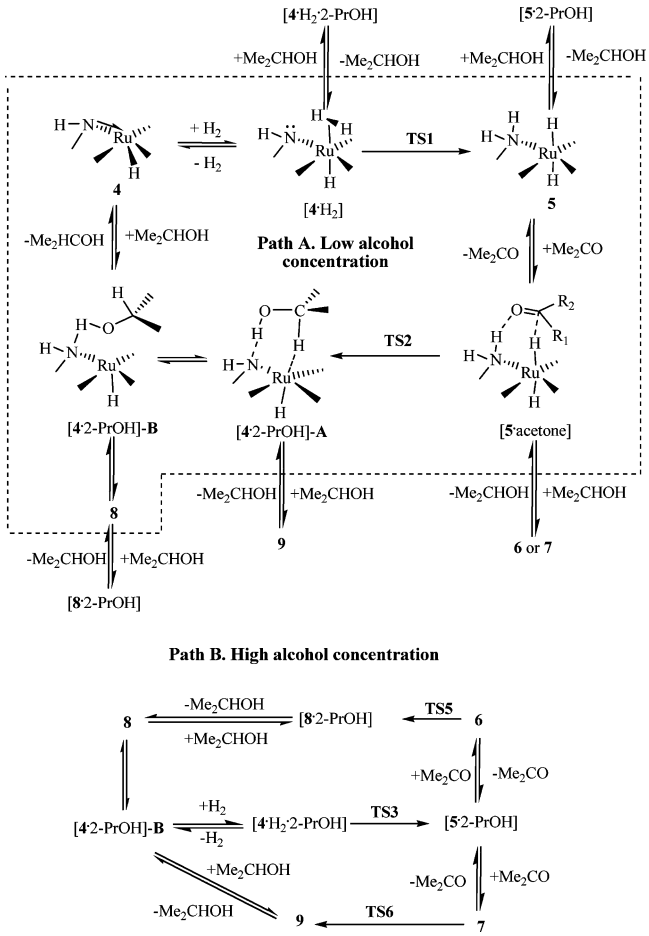

catalysts for H_2 transfer to ketones, but the alcohol assistance of H_2 transfer could also account for these variations.

On the basis of the experimental and theoretical results, we propose an expanded mechanism for catalysis shown in Scheme 9. It includes both an alcohol-free pathway (path A, the domain within the dotted lines) that operates in the benzene solutions at low alcohol concentrations and an alcohol-assisted pathway (path B) for high alcohol concentrations and/or solutions in alcohol. Path A has been described previously apart from the intermediate [**4**·2-PrOH]-**B**, an alcohol adduct of the amidohydridoruthenium complex **4**. Path B circles around outside of the dotted line domain, where additional 2-PrOH is present. It includes the alcohol-assisted H_2 splitting step **TS3**, two possible alcohol-assisted hydrogenations of the ketone via **TS5** or **TS6**, and the formation of alkoxide intermediates **8** and **9**.

Conclusions

The design and synthesis of a novel appH ligand, lacking α-hydrogens, which is an analogue of 2-(aminomethyl)pyridine, permits the isolation of a stable amidohydrido complex, RuH-(*S*-binap)(app) (**3**). It is prepared from a parent chloro-hydrido complex, RuHCl(*S*-binap)(appH) (**2**), by dehydrochlorination by use of the strong base KO^{t}Bu. The crystal structure of **3** reveals the presence of a short Ru−N(amido) bond and a trigonal-planar geometry around the amido nitrogen. Like similar amido complexes previously reported,[13,47] amido **3** is an active catalyst for hydrogenation of ketones without a base added. The substrate-reducing complex is likely to be *trans*-RuH_2(*S*-binap)-(appH) according to our calculations and by analogy with other

similar systems,[13,33] but the formation of this dihydride is unfavorable entropically and has not yet been observed. A kinetic study in benzene shows that systems using **3** as a catalyst behave differently from other diamine systems such as *trans*-$Ru(H)_2$(*R*-binap)(tmen), $Ru(H)_2(PPh_3)_2$(*R*,*R*-dach), $RuH(PPh_3)_2$-($H_2NCMe_2CMe_2NH$), and $RuHCl(PPh_2C_6H_4CH_2NHC_6H_{10}$-$NHCH_2C_6H_4PPh_2)$.[13,33,47] While the measured rates in all cases show a dependence on both Ru and H_2 concentration, the rate of catalysis with **3** is also a function of the product concentration and therefore is autocatalytic.

That indeed the product affects the hydrogenation rate was confirmed by adding *rac*-1-phenylethanol to the reaction mixture prior to the hydrogenation. The addition of 2-propanol also increases the rate, but not as much as PhCH(OH)Me. Moreover, the highest rate and TOF were achieved when 2-propanol was used as solvent. These findings have been explained by a second pathway, the alcohol-assisted H_2 splitting mechanism in which added alcohol lowers the energy of this rate-limiting step. This alcohol effect has been observed previously in other metal−ligand bifunctional catalysis. It seems to be more pronounced for the aminomethylpyridine type of ligands than simple diamines. The reason for this different behavior is not clear. One possible explanation is the decrease in steric bulk on one side of amine ligand due to the planarity of the pyridine ring. This might also explain why the use of this type of pyridine ligand is so effective in the hydrogenation of bulky ketones.[34] The gas-phase DFT calculations support the experimental results. We find that the rate-limiting step is the heterolytic cleavage of H_2 by the Ru amido complex with the following parameters: $\Delta G^{\ddagger} = 19.7$ kcal mol^{-1}, $\Delta H^{\ddagger} = 9.93$ kcal mol^{-1}, $\Delta S^{\ddagger} = -32.7$ cal mol^{-1} K^{-1}. The presence of alcohol significantly lowers the activation barrier for this process by about 5 kcal/mol in free energy ($\Delta G_a^{\ddagger} = 14.7$ kcal mol^{-1}, $\Delta H_a^{\ddagger} = -5.81$ kcal mol^{-1}, $\Delta S_a^{\ddagger} = -68.7$ cal mol^{-1} K^{-1} in the case of 2-PrOH) but not enough to bring it below the hydrogenation step ($\Delta G_{hyd}^{\ddagger} = 8.7$ kcal mol^{-1}, $\Delta H_{hyd}^{\ddagger} = -4.7$ kcal mol^{-1}, $\Delta S_{hyd}^{\ddagger} = -76.6$ cal mol^{-1} K^{-1}). We have also investigated two alcohol-assisted mechanisms of ketone H_2-hydrogenation in 2-propanol solvent. These can explain the differences in enantioselectivity observed between the hydrogenations in benzene and 2-propanol because of the different orientations of the substrate molecule in the transition states **TS2** versus **TS5** and **TS6**. They also indicate that alkoxide complexes are the catalyst resting states. These pathways may be broadly applicable to other Noyori-type catalyst systems.

This report has also introduced the direct synthesis of RuHCl-(binap)(appH) from $RuCl_2$(binap)(PPh_3) according to Scheme 5. This is proving to be a valuable route for the synthesis of a variety of other ruthenium precatalysts.

Experimental Section

General Considerations. Unless otherwise stated, all the operations were carried out under an inert atmosphere using standard Schlenk and glovebox techniques. **1a**, **1b**,[37] $RuCl_2(PPh_3)_2$,[60] and $RuCl_2$(*S*-binap)(PPh_3)[41] were prepared according to the literature procedures. THF, diethyl ether, hexanes, and benzene were dried and distilled from sodium benzophenone ketyl under an argon atmosphere. 2-Propanol and methanol were dried and distilled from Mg/I_2 also under Ar. Acetophenone was dried over molecular sieves and distilled under an argon atmosphere. Deuterated solvents were purchased from Cambridge Isotope Laboratories and degassed and dried over molecular sieves prior to use. All other reagents were purchased from Sigma-Aldrich and used without further purification. The ^{1}H and ^{13}C NMR spectra were recorded on a Mercury 400 spectrometer operating at 400 MHz for ^{1}H and 100 MHz for ^{13}C. The ^{31}P NMR spectra were obtained on a Gemini 300 spectrometer (121.5 MHz). The ^{1}H and ^{13}C NMR were measured relative to partially deuterated solvent peaks but are reported relative to tetramethylsilane. The ^{31}P chemical shifts are reported relative to 85% H_3PO_4 as an external reference. The elemental analysis was performed at the Department of Chemistry, University of Toronto, on a Perkin-Elmer 2400 CHN elemental analyzer.

The catalytic hydrogenations and the kinetic measurements were performed under constant pressures of H_2 gas in a 50 mL Parr high-pressure reactor. A constant temperature for these experiments was maintained using a Fisher Scientific IsoTemp 1016D water bath. The samples were analyzed by chiral GC on a Perkin-Elmer Autosystem XL with a Chrompack capillary column (ChirasilDEX CB 25 m × 0.25 mm). Hydrogen was used as a carrier gas at a column pressure and temperature of 5 psi and 130 °C, an injector temperature of 250 °C, and an FID temperature of 275 °C. The retention times were as follows: acetophenone, 5.20 min; (*R*)-1-phenylethanol, 8.95 min; and (*S*)-1-phenylethanol, 9.50 min.

Synthesis of *N*-(2-(Pyridin-2-yl)propan-2-yl)acetamide, 1c. Potassium hydroxide (4 g, 0.07 mol) and **1b** (0.7 g, 2.7 mmol) were dissolved in 40 mL of dry methanol under an argon atmosphere. This solution was then added to 1.4 g of Raney nickel in 10 mL of dry methanol. This was placed under 1 atm of H_2 and stirred for 4 h. The mixture was then filtered through a pad of Celite and the solvent from the filtrate evaporated *in vacuo*. Distilled water (10 mL) was added to the yellowish residue and the mixture extracted with $CHCl_3$ (3 × 10 mL). The combined organic layers were dried over $MgSO_4$. Removal of the solvent gave a pale yellow solid. Yield: 0.32 g (65%). ^{1}H NMR (400 MHz, $CDCl_3$, δ): 1.72 (s, 6H, $-CH_3$), 2.01 (s, 3H, $-CH_3$), 7.15 (ddd, $J_{HH} = 7.6$, 4.8, 1.2 Hz, 1H, py), 7.36 (m, 1H, py), ca. 7.66 (s, br, 1H, NH), 7.67 (dt, $J_{HH} = 7.2$, 1.6 Hz, 1H, py), 8.47 (m, 1H, py). ^{13}C NMR (100 MHz, $CDCl_3$, δ): 24.85, 27.66, 56.66, 119.67, 122.02, 137.25, 147.77, 164.76, 169.56. EI-MS (*m*/*z*): 178 (M^+, 25%), 163 (35%), 135 (65%), 121 (100%).

Synthesis of 2-Amino-2-(2-pyridyl)propane (appH). A yellow solution of **1c** (0.3 g, 1.7 mmol) in 6 M HCl (40 mL) was refluxed in air overnight. The cooled reaction mixture was made strongly basic (pH 10 against universal pH paper) with 30% NaOH. This was extracted with $CHCl_3$ (3 × 10 mL). The organic extracts were dried over $MgSO_4$, and the solvent was removed *in vacuo*, leaving the product as a pale brown oil. Yield: 0.21 g (91%). The ligand was used without further purification. ^{1}H NMR (400 MHz, $CDCl_3$, δ): 1.45 (s, 6H, $-CH_3$), 1.88 (s, br, 2H, $-NH_2$), 7.06 (m, 1H, py), 7.4 (d, br, $J = 7.6$ Hz, 1H, py), 7.58 (dt, $J = 7.6$, 1.4 Hz, 1H, py), 8.50 (s, br, 1H, py). ^{13}C NMR (100 MHz, $CDCl_3$, δ): 31.37, 54.14, 118.53, 121.40, 136.53, 148.76, 168.32. EI-MS (*m*/*z*): 137 (M^+, 25%), 121 (100%), 104, (35%), 80 (20%), 58 (95%).

Synthesis of Ru(H)Cl(*S*-binap)(appH), 2. Triethylamine (0.11 g, 1 mmol, 0.15 mL) was added to a suspension of $RuCl_2$(*S*-binap)-(PPh_3) (0.58 g, 0.55 mmol) in 8 mL of dry THF in a 50 mL Schlenk flask under an H_2 atmosphere. The reaction was stirred for 4 h at room temperature, resulting in a deep red solution. After purging the flask with argon, neat appH (0.09 g, 0.6 mmol) was added and stirring continued for 1 h. The solvent from the resulting intense orange-yellow solution was removed *in vacuo*. The solids were extracted with a minimum amount of dry THF and filtered to remove the insoluble $[Et_3NH]Cl$ salt. The addition of the 1:1 hexanes/ether mixture precipitated the orange-yellow product. The solids were filtered off, washed with a hexanes/ether mixture, and vacuum-dried. Yield: 0.35 g (70%). Anal. Calcd: C, 69.30; H, 5.71; N, 2.89. Found: C, 69.02; H, 5.75; N, 2.97. ^{1}H NMR (thf-d_8, δ), major isomer: −15.79 (dd, $^2J_{HP} = 28$ and 24.5 Hz, 1H, RuH), 1.46 (s, 3H, $-CH_3$), 1.84 (s, 3H, $-CH_3$), 2.7 (bd, 1H, NH,

(60) Hollan, P. A.; Stephenson, T. A.; Wilkinson, G. *Inorg. Synth.* **1970**, *12*, 237−240.

$^2J_{HH}$ = 9.6 Hz), 3.4 (bd, 1H, NH, $^2J_{HH}$ = 9.6 Hz), 6.2−8.4 (m, 36H); minor isomer: −16.28 (dd, $^2J_{HP}$ = 29.8 and 21.7 Hz, RuH), 1.22 (s, $-CH_3$), 1.52 (s, $-CH_3$). $^{31}P\{^1H\}$ NMR (thf-d_8, δ), major isomer: 66.2 (d, $^2J_{PP}$ = 39.4 Hz), 72.1 (d); minor isomer: 62.3 (d, $^2J_{PP}$ = 41.4 Hz), 68.7 (d). ^{13}C NMR (thf-d_8, δ): 28.66, 31.8, 62.22, 119.36, 122.02, 124.91, 125.6, 125.76, 126.13, 126.57 (m), 127.67 (m), 127.92, 128.25, 128.4, 128.5, 128.9, 129.2, 129.4, 129.5, 133.87, 134.6, 134.73, 135.45, 136.69, 136.79, 138.76, 138.82. IR (Nujol, cm^{-1}): 1995 (ν_{RuH}), 3329, 3402 (ν_{NH}).

Synthesis of RuH(*S*-binap)(app), 3. Ru(H)Cl(S-binap)(appH) (0.260 g, 0.28 mmol) was placed in a 25 mL Schlenk flask and dissolved in 4 mL of dry THF under an argon atmosphere. The solid KO^{t}Bu (0.08 g, 0.7 mmol) was added to this orange-yellow solution, immediately turning its color deep red. The reaction was stirred for 40 min, and THF was removed *in vacuo*. Solids were extracted with approximately 1 mL of dry THF and filtered through a pad of Celite. Hexanes (7 mL) were added to the filtrate, precipitating a red product, which was filtered, washed with hexanes, and vacuum-dried. Yield: 0.20 g (78%) ^1H NMR (C_6D_6, δ): −15.46 (dd, $^2J_{HP}$ = 26.1 and 40 Hz, 1H, RuH), 1.34 (s, 3H, $-CH_3$), 1.57 (s, $-CH_3$), 4.3 (d, $^3J_{HP}$ = 4.3 Hz, 1H, NH), 5.7 (m, 1H), 6.6 − 8.8 (m, 35 H). $^{31}P\{^1H\}$ NMR (C_6D_6, δ): 71.0 (d, $^2J_{PP}$ = 31 Hz), 82.7 (d). ^{13}C NMR (C_6D_6, δ): 33.87, 35.42, 72.67, 120.03, 120.35, 125.30, 125.60 (m), 125.7−129.3 (peaks covered due to the NMR solvent), 133.3, 133.54, 134.5 (m), 137.8, 139.3, 139.6, 140.07, 140.42, 142.62, 143.04, 144.2, 144.68, 155.74, 174.24. IR (Nujol, cm^{-1}): 1903 (ν_{RuH}), 3234 (ν_{NH}). Several attempts to obtain a satisfactory elemental analysis on the crystalline, spectroscopically pure product failed due to the high sensitivity of this complex to air and nitrogen and difficulties with combustion. The typical result: Anal. Calcd: C, 73.07; H, 5.69; N, 3.10. Found: C, 69.35; H 5.42; N, 2.82.

Catalytic Tests with 2 and 3. A solution containing acetophenone (0.250 g, 2.1 mmol) and precatalyst **2** (7 mg, 7.5 × 10^{-6} mol) was dissolved in 5 mL of benzene. This solution was injected in a high-pressure reactor under the H_2 gas previously thermostated at 20 °C. This was followed by the addition of a KO^{t}Bu (0.021 g, 0.19 mmol) suspension in 0.2 mL of benzene. After the addition of the base, the H_2 pressure was set to 10 atm. The same procedure was followed for the catalytic reaction with **3** except the base was not added.

Kinetic Measurements. The standard solutions of **3** (1.5 mM) and acetophenone (0.833 M) were prepared by dissolving a required amount of a compound in 5 mL of benzene or 2-propanol. The fresh solution of **3** was prepared before each run. The reaction mixtures were prepared by pipetting the required volumes of the standard solutions and benzene or 2-propanol. For the runs in which they were used as additives, the alcohols (racemic 1-phenylethanol and 2-propanol) were added in required amounts to the acetophenone standard solution so that, after the dilution, the concentration of *rac*-1-phenylethanol was 0.04 M and for 2-propanol 0.06 M. For all the runs the solution of acetophenone, followed by the solution of **3**, was injected into the already thermostated reactor under the desired pressure of H_2 to give the final reaction volume of 5 mL. The reaction time was measured from the addition of complex **3** solution. The samples were withdrawn from the reactor at regular time intervals of 5 min. The sampling took about 10 s, during which time the pressure in the reactor fell to almost atmospheric. The samples taken were analyzed by chiral GC. The transfer hydrogenation experiment was carried in an argon glovebox in well-sealed and stirred 10 mL round-bottom flask.

X-ray Structure Determination of 3. Single crystals of Ru(H)(*S*-binap)(app)·$0.5C_6H_{14}$ were grown by a slow diffusion of hexanes into a concentrated solution of the complex in benzene. The data were collected using a Nonius Kappa-CCD diffractometer at 150 K with Mo Kα (λ = 0.71073 Å) and integrated and scaled using the Denzo-SMN package. SHELEX V6.10 was used to solve and refine the structure by direct methods. The hydride ligand was located and refined with isotropic thermal parameters. The crystallographic data are summarized in Table 3. Refinement of data revealed the presence of solvent molecules in the unit cell that refined the best as 2-methylpentane with an occupancy of 1/2 for all the solvent atoms.

Table 3. Summary of X-ray Parameters for Complex 3

empirical formula	$C_{52}H_{44}N_2P_2Ru\cdot0.5C_6H_{14}$
fw	902.99
temperature, K	150(2)
wavelength, Å	0.71073
cryst syst	monoclinic
space group	$P2_1$
a, Å	11.139(2)
b, Å	12.076(2)
c, Å	16.788(3)
α, deg	90
β, deg	95.22(3)
γ, deg	90
volume, $Å^3$	2248.7(8)
Z	2
density (calcd), g cm^{-3}	1.334
absorp coeff, mm^{-1}	0.459
F(000)	938
cryst size, mm	0.44 × 0.40 × 0.38
range, θ ,deg	2.91−27.49
no. of reflns collected	23 147
no. of indep reflns	9593 [*R*(int) = 0.0453]
completeness to θ = 27.49°	99.1%
refinement method	full-matrix least-squares on F^2
goodness-of-fit on F^2	1.070
final *R* indices [$I > 2\sigma(I)$]	R1 = 0.0431, wR2 = 0.1114
R indices (all data)	R1 = 0.0482, wR2 = 0.1156
largest diff peak and hole, e $Å^{-3}$	1.212 and −0.943

Computational Details. All DFT calculations were performed using Gaussian 03 (Revision D.01)[61] using a restricted hybrid mPW1PW91 functional[52,53] with SDD[54] ECP (GenECP) for ruthenium and 6-311++G(d,p) level for nonmetallic elements using a default grid. The synchronous transit-guided quasi-Newton (STQN) method (QST2) was used for the optimization of transition states.[62] All transition states had one imaginary frequency, consistent with the reaction course. The reported energies are for gas phase at 298.15 K and 1 atm and are corrected for zero-point energies but uncorrected for the translation and rotation.

Acknowledgment. This work was supported by grants to R.H.M. from NSERC Canada and PRF as administered by American Chemical Society. Digital Specialty is thanked for a gift of *S*-binap. We thank Prof. Dmitri Goussev for information on DFT calculations.

Supporting Information Available: The rate law for the hydrogenation of acetophenone in benzene with **3** as a catalyst obtained by numerical integration of the data from the Figures 2 and 3. X-ray structural data and crystallographic file (CIF) for complex **3**. XYZ coordinates for all the optimized structures and the calculated energies. This material is available free of charge at http://pubs.acs.org.

OM700849W

(61) Frisch, M. J.; et al. *Gaussian 03*, Revision C.02 ed.; Gaussian Inc.: Wallingford, CT, 2004. See the Supporting Information for the complete author list.

(62) Peng, C.; Ayala, P. Y.; Schlegel, B. H.; Frisch, M. J. *J. Comput. Chem.* **1996**, *17*, 49−56.